Journal of Marine Science and Engineering

MDPI

Article

Impacts of Atmospheric Pressure on the Annual Maximum of Monthly Sea-Levels in the Northeast Asian Marginal Seas

MyeongHee Han [1], Yang-Ki Cho [1,*], Hyoun-Woo Kang [2], SungHyun Nam [1], Do-Seong Byun [3], Kwang-Young Jeong [3] and Eunil Lee [3]

1 School of Earth and Environmental Sciences/Research Institute of Oceanography, Seoul National University, Seoul 08826, Korea; skiing1@snu.ac.kr (M.H.); namsh@snu.ac.kr (S.N.)
2 Ocean Circulation & Climate Research Center, Korea Institute of Ocean Science & Technology, Busan 49111, Korea; hwkang@kiost.ac.kr
3 Ocean Research Division, Korea Hydrographic and Oceanographic Agency, Busan 49111, Korea; dsbyun@korea.kr (D.-S.B.); kwangyoung@korea.kr (K.-Y.J.); elee@korea.kr (E.L.)
* Correspondence: choyk@snu.ac.kr; Tel.: +82-2-880-6749; Fax: +82-2-872-3269

Received: 19 May 2020; Accepted: 7 June 2020; Published: 10 June 2020

Abstract: Monthly mean sea-levels have annual maxima in August in the northeast Asian marginal seas (NEAMS). Based on satellite altimetry data, the rising rate of the August NEAMS sea-level (ANS, 4.2 mm·yr^{-1}) is greater than those of the NEAMS (3.6 mm·yr^{-1}) and global (3.4 mm·yr^{-1}) annual mean sea-levels. Thus, the interannual variations of ANS are classified as relatively high (period H) and low (period L) years and have been analysed because of the high risk of sea-level fluctuation to the coastal regions in August. In period H, there are large atmospheric pressure gradients between the high pressure zone in the Kuroshio Extension (KE) and the low pressure zone in the west of Taiwan (WT). In period L, the atmospheric pressure gradients are small between the above-mentioned zones. Large atmospheric pressure gradients induce strong west-northwestward wind stresses and more Ekman transport from the northwest Pacific Ocean into the NEAMS. The correlation coefficient between August NEAMS sea-level index (ANSI), which is the difference of atmospheric pressure anomalies between the KE and the WT, and the August NEAMS sea-level anomaly (ANSA) is 0.73. Although there is a significant correlation (coefficient: 0.64) between ANSA and the East Asian summer monsoon index (EASMI), ANSI might be more useful in estimating the variability of ANSA.

Keywords: sea-level; interannual variation; August NEAMS sea-level index; atmospheric pressure; wind stress; Ekman transport; satellite altimetry

1. Introduction

Sea-level rising due to climate change is seriously threatening the lives of human beings [1]. Sea-level changes can be largely affected by barometric, steric, and mass components [2]. Although there are many ongoing studies on sea-level rise caused by thermal expansion and ice sheet melting [3,4], there are few studies on the impacts of wind stress by atmospheric pressure distributions on sea-level variation in marginal seas.

The Yellow Sea (YS), East China Sea (ECS), and East/Japan Sea (EJS) make up the northeast Asian marginal seas (NEAMS), which are surrounded by Korea, China, Russia, Japan, and Taiwan. The NEAMS are connected to the Pacific Ocean through narrow straits and shallow continental shelves (Figure 1). The sea-level responds immediately to external forcing by quickly propagating barotropic waves in the NEAMS [5–7]. Temporal variations of volume transport in the Korea Strait (KS), a major strait in the NEAMS, is influenced significantly by along-strait wind stresses, atmospheric pressures,

and sea-level differences between the Pacific and the EJS for timescales longer than 100 days [7]. The surface wind stress plays an important role in both the volume transport and sea-level changes in the marginal seas [8–10]. The effect of the zonal wind stress on the meridional migration of a subpolar front in the EJS has been previously reported [11]. The wind stress along the east coast of Sakhalin, an island in the north of Soya Strait (SS), induces interannual variation of volume transport along the SS [12]. The interannual variation of the mean sea-level in the ECS is linked to the surface wind stress in the North Pacific [9]. Wind stress and atmospheric pressure were proposed as potential causes of the large seasonal variation of sea-level [13].

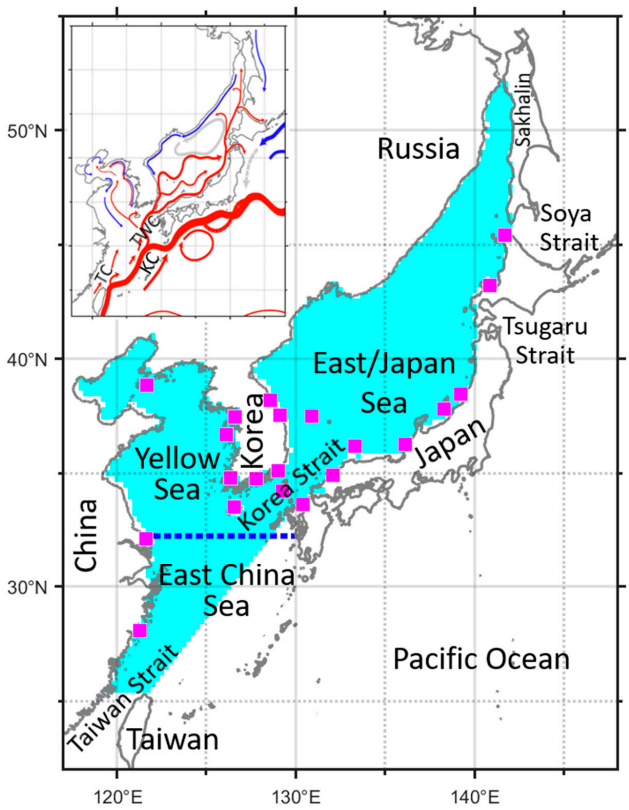

Figure 1. Domain of the northeast Asian marginal seas (NEAMS, cyan) and locations of twenty-one tide-gauge stations (magenta squares, available from https://www.psmsl.org). The blue dotted line along the 32.25° N between China and Japan is for meridional Ekman transports. Schematics of the regional circulation patterns, with major surfaces (red or blue) and intermediate (grey) currents transporting warm (red) and cold (blue) waters in the upper left box (available from http://www.khoa.go.kr). The stronger currents are shown with thicker arrows, while continuous and continual currents are indicated by solid and dashed arrows, respectively. KC, TC, and TWC are the Kuroshio Current, and the Taiwan and the Tsushima Warm Currents, respectively.

Moreover, the effect of typhoons, which induce high sea-levels and frequently occur in the NEAMS in August, needs to be studied. The sea-level maxima and their interannual variations in August need to be understood so that issues such as coastal flooding, saltwater intrusion, and habitat destruction, can be prepared beforehand [14]. Sea-level changes in the YS, ECS, and EJS have been reported, mainly with tide-gauge and altimetry measurements [15], but the causes and dynamics of August sea-level changes in the NEAMS are yet to be studied.

In this study, we try to understand the mechanism of the interannual NEAMS sea-level variability caused by atmospheric pressure and wind stress in August. The data and methods are presented in Section 2, and the results and discussion are described in Sections 3 and 4, respectively. Conclusions are presented in Section 5.

2. Data and Methods

Monthly mean sea-levels in August in the NEAMS were analysed from 1993 to 2018. The daily absolute dynamic topography (ADT) data provided by the Copernicus Marine Environment Monitoring Service (CMEMS) were gridded with a horizontal resolution of 0.25° from all satellite altimeter missions. ADT is the sum of sea-level anomalies and the mean dynamic topography (mean sea-level driven by thermodynamic processes in the ocean, [16,17]). We used level four of the ADT data (e.g., dt_global_allsat_phy_l4_20180831_20190101.nc) downloaded by ftp from the CMEMS portal [18,19]. More information regarding ADT is available on the CMEMS web site [20].

Monthly mean sea-level data at twenty-one tide-gauge stations (magenta squares in Figure 1), from 1993 to 2018, were provided by the Permanent Service for Mean Sea Level [21,22]. The sea-level data are from stations in Korea (nine stations: INCHEON, ANHEUNG, MOKPO, JEJU, YEOSU, BUSAN, MUKHO, SOKCHO, ULLEUNG), China (three stations: KANMEN, LUSI, and DALIAN), and Japan (nine stations: HAKATA, IZUHARA II, HAMADA II, SAIGO, MIKUNI, OGI, AWA SIMA, OSHORO II, WAKKANAI). The inverted barometer effect was removed from the sea-level observed at the tide-gauge stations with the assumption that 1 hPa atmospheric pressure decreases the water level by 1 cm [23,24]. The tide-gauge data, after removing the inverted barometric effect, were matched to have the same mean sea-level as the satellite altimetry data in August for over 26 years (Figure 2b).

Monthly mean sea-level atmospheric pressure and surface wind stress data from the European Centre for Medium-Range Weather Forecasts (interim reanalysis) were used with a horizontal resolution of 0.75° over 26 years (1993–2018) around the NEAMS.

The linear trend over the time period (26 years) was removed to investigate the interannual variation. The Ekman transport, per unit width, within the surface Ekman layer (VT_{Ekman}, m^2 s^{-1}) was calculated using Equation (1):

$$\begin{aligned} VT_{Ekman} &= \int_{D_{Ekman}}^{0} u_{Ekman}\, dz = \int_{D_{Ekman}}^{0} \frac{1}{f\rho}\frac{\partial \tau}{\partial z} dz = \frac{1}{f\rho}\left[\,\tau\,\right]_{D_{Ekman}}^{0} \\ &= \frac{1}{f\rho}\left\{\,\tau\,(z=0) - \tau\,(z=D_{Ekman})\,\right\} = \frac{\tau\,(z=0)}{f\rho} \end{aligned} \tag{1}$$

Here, u_{Ekman}, D_{Ekman}, $f\ (= 2\Omega \sin\varphi)$, Ω ($\approx 7.2921 \times 10^{-5}$), φ, ρ, z, and τ denote the Ekman velocity (m s^{-1}), Ekman depth (m), Coriolis parameter (rad s^{-1}), rotation rate of the Earth (rad s^{-1}), latitude, density of sea water ($\approx$1025 kg m^{-3}), depth (m), and wind stress (N m^{-2}), respectively.

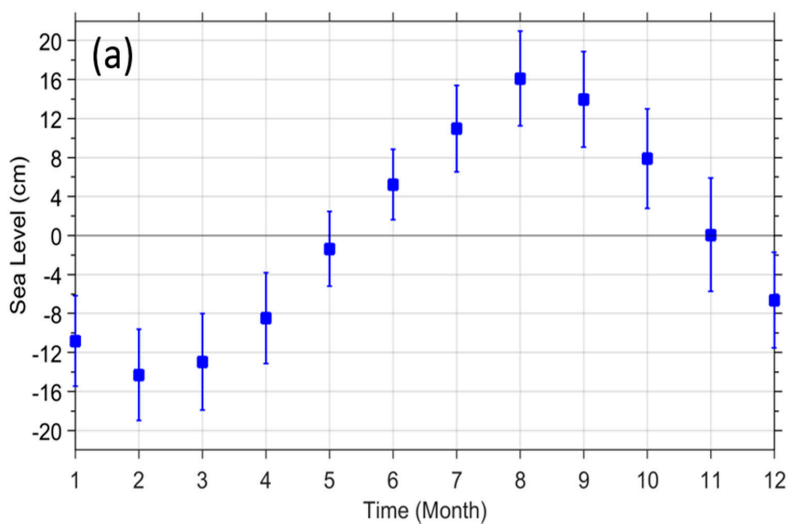

Figure 2. *Cont.*

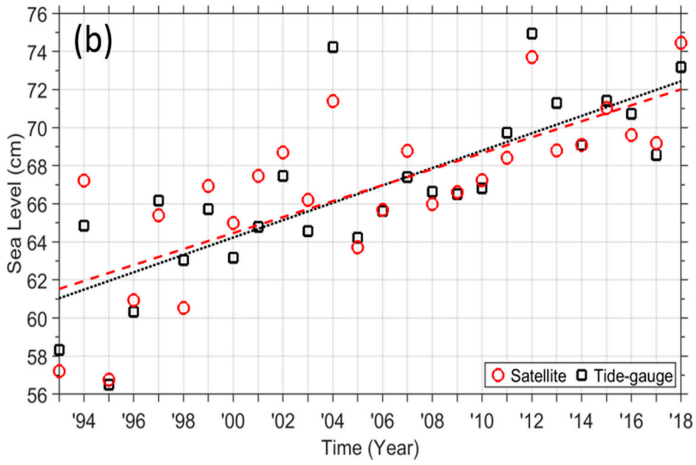

Figure 2. (**a**) Climatology of de-trended monthly mean NEAMS sea-levels from tide-gauge observations averaged from 1993 to 2018. 0 cm represents the trend line of the original tide-gauge data and the inverted barometer effect was not removed. The maximum and minimum are in August and February, respectively. Error bars indicate the positive and negative standard deviations of monthly sea-level for 26 years from climatology. (**b**) Time-series of August mean NEAMS sea-levels from satellite altimetry (red open circles) and tide-gauge observations (black open squares) from 1993 to 2018 after removing the inverted barometer effect. The vertical reference datum (0 cm) of the tide-gauge data had been adjusted to have the same mean sea-level in August for 26 years between tide-gauge data and satellite altimetry, and the dashed red and black dotted lines represent their trends.

3. Results

3.1. Long-Term Trend of Sea-Levels in August

The mean seasonal variation of twenty-one tide-gauge observations was examined without removing the inverted barometer effect and averaged from 1993 to 2018 in order to determine annual variations of the actual sea-level. Maximum and minimum of de-trended sea-levels are +16.1 cm in August and −14.3 cm in February, respectively (Figure 2a). Rising rates of sea-levels in August, from satellite altimetry (4.2 mm·yr^{-1}) and tide-gauge observations (4.6 mm·yr^{-1}), after removing the inverted barometer effect from 1993 to 2018, are compared in Figure 2b (dashed red and dotted black, respectively). Even though there are several causes of these different rising rates (0.4 mm·yr^{-1}), including uneven distributions of tide-gauge stations, the variations of the two datasets are similar. Sea-level data from satellite altimetry and from tide-gauge observations, which are independent of each other, have a strong positive correlation with coefficients of 0.95 (August, p-value < 0.01) and 0.97 (annual, p-value < 0.01, not shown), respectively.

3.2. Interannual Variation of Sea-Level Anomalies in August

The interannual variations of the August NEAMS sea-level anomalies (ANSA) from satellite altimetry are classified as years of relatively high (positive anomalies above +2 cm) and low (negative anomalies below −2 cm) sea-levels; period H (1994, 1999, 2001, 2002, 2004, 2012, and 2018) and period L (1993, 1995, 1996, 1998, and 2005), respectively (Figure 3). The selected threshold of 2 cm is the accuracy of TOPEX/Poseidon's radar altimeter [25]. The wind stress and Ekman transport in Section 3.3 and sea-level atmospheric pressure in Section 3.4 were analysed to determine the positive and negative effects of atmospheric conditions on ANSA based on the periods H and L. We will hereafter use ANSA from satellite altimetry data only.

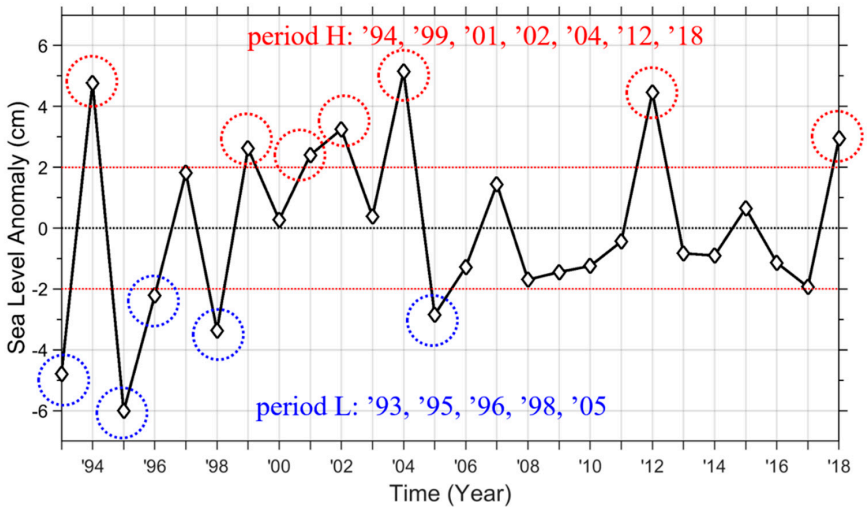

Figure 3. Time-series of the de-trended August sea-level anomalies averaged over the NEAMS from 1993 to 2018 are classified as seven high (higher than +2 cm) and five low (lower than −2 cm) years. Period H (1994, 1999, 2001, 2002, 2004, 2012, and 2018) and period L (1993, 1995, 1996, 1998, and 2005) are represented by red and blue dotted circles, respectively. 0 cm here is the trend of August sea-level, the same as the red dashed line in Figure 2b.

3.3. Ekman Transport and Sea-Level Anomaly

The ECS is the main path for the Taiwan and the Tsushima Warm Currents which are the primary seawater advection sources in the NEAMS [26]. The meridional Ekman transport anomaly from the east coast of China to the west coast of Japan along 32.25° N in the ECS (blue dotted line in Figure 1) was calculated to examine the relationship between wind stress and ANSA. The correlation between the meridional Ekman transport anomaly along 32.25° N in August and ANSA, from 1993 to 2018, is significant (correlation coefficient 0.69 with p-value < 0.01, Figure 4). Thus, the Ekman transport anomaly by the wind stress in the southern NEAMS and the sea-level anomaly in the NEAMS are closely related in August.

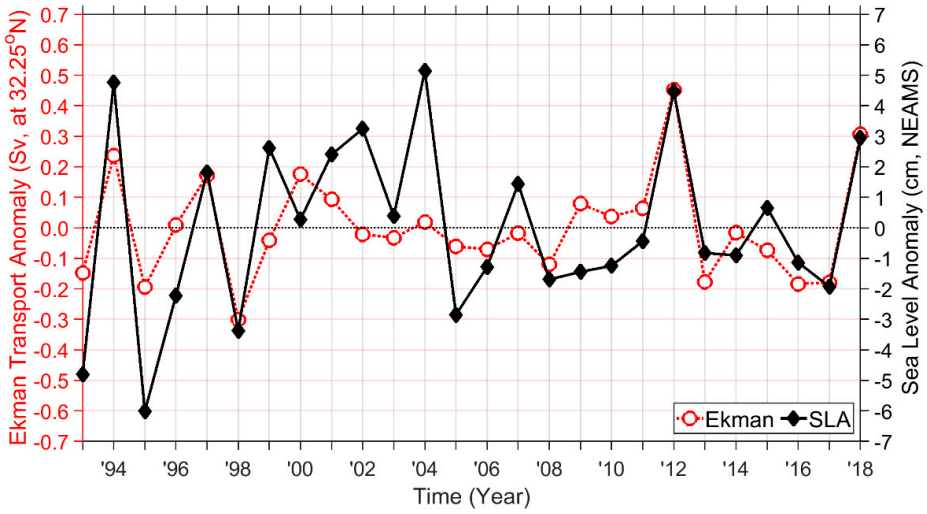

Figure 4. Time-series of the meridional Ekman transport anomaly, along the 32.25° N (blue dotted line in Figure 1) from the east coast of China to the west coast of Japan (dotted red), and the de-trended mean sea-level anomalies averaged over the NEAMS (solid black) from satellite altimetry data in August from 1993 to 2018. The correlation coefficient between the sea-level anomaly and the meridional Ekman transport anomaly is 0.69 (p-value < 0.01).

There are strong west-northwestward wind stresses in the south of the NEAMS for the period H around 136° E and 29° N in Figure 5a and weak west-northwestward wind stresses in the south of the NEAMS for the period L around 140° E and 28° N in Figure 5b. The Ekman transport can be calculated by using Equation (1) to examine the relationship between wind stress and the sea-level change. More north-northeastward Ekman transport by strong west-northwestward wind stress brings more seawater from the northwest Pacific Ocean into the NEAMS, and less north-northeastward Ekman transport by weak west-northwestward wind stress brings less seawater into the NEAMS. The directions of wind stresses in the ECS are westward and west-northwestward, which can induce more Ekman transport into the YS and EJS for the period H in Figure 5a. These directions of wind stresses result from the expansion of the high and the low pressures westward and eastward, respectively for the period H. On the contrary, the directions of wind stresses in the ECS are almost northward, which cannot cause Ekman transport into the YS and EJS for the period L in Figure 5b. The northward directions of wind stresses are due to the westward retreat of the low pressure in the south of the NEAMS for the period L.

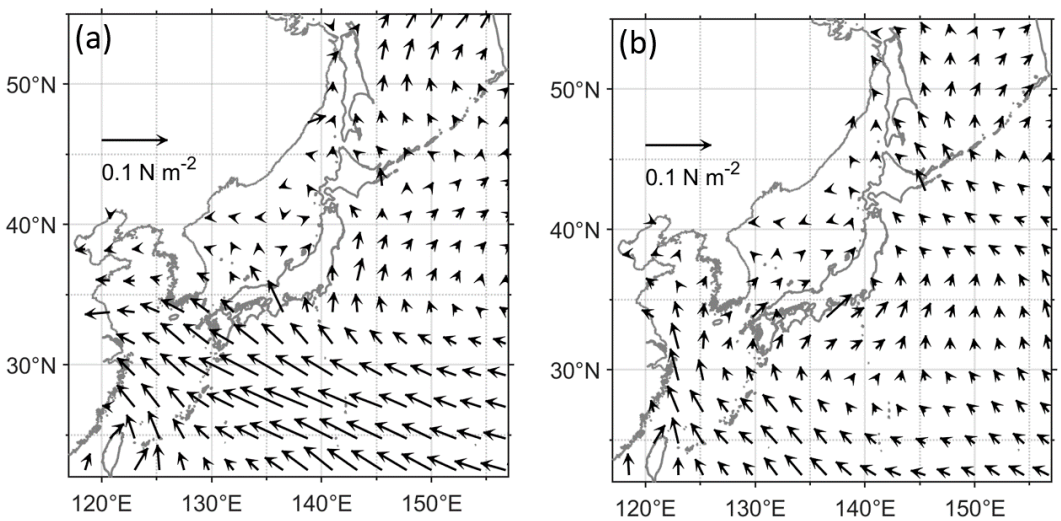

Figure 5. Surface wind stress (black vector) in August averaged for periods (**a**) H and (**b**) L. There are strong (weak) west-northwestward wind stresses around 136° E and 29° N (140° E and 28° N) in the south of the NEAMS for the period H (period L). Coastlines are drawn in grey.

The Ekman transports per unit width were calculated based on Equation (1) and their anomalies are plotted in Figure 6a,b. The directions of Ekman transport anomalies in the southern NEAMS are northward for the period H as shown in Figure 6a, and they are southward for the period L as shown in Figure 6b. The positive sea-level anomaly is due to more northward Ekman transport in the south of the NEAMS for the period H in Figure 6a, and the sea-level anomaly from the satellite observations in Figure 6c is similar to that. The negative sea-level anomaly is due to less northward Ekman transport in the south of the NEAMS for the period L in Figure 6b, and the result of the satellite observation is similar to that in Figure 6d.

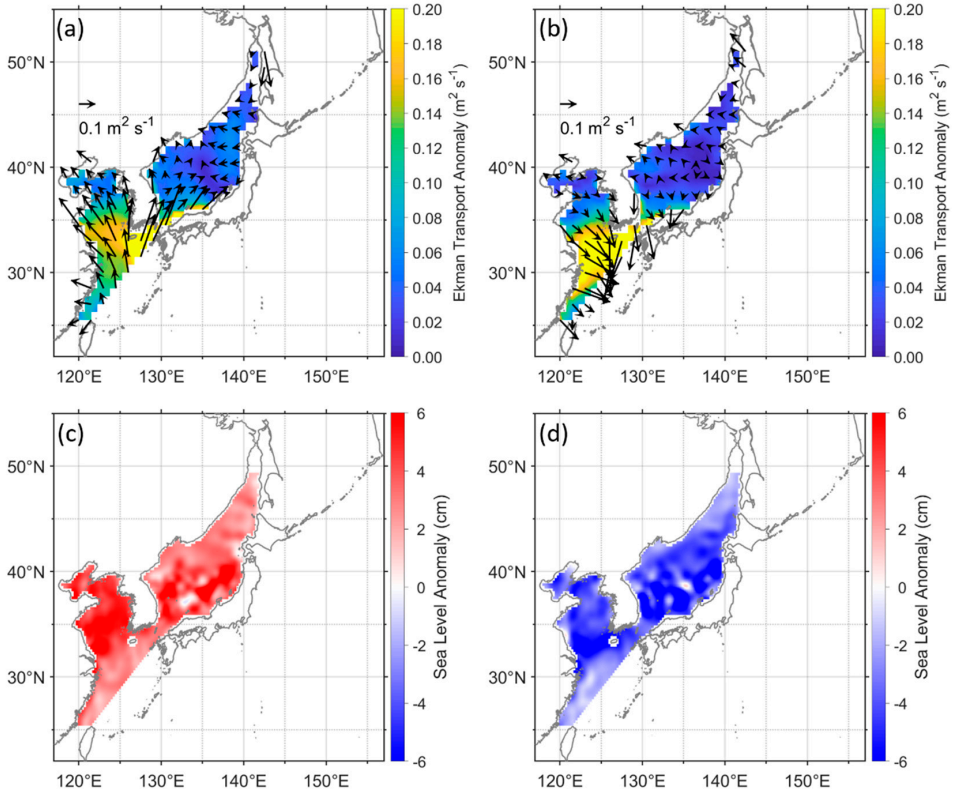

Figure 6. The Ekman transport anomaly per unit width based on Equation (1) during the periods (**a**) H and (**b**) L. The strength and direction of the Ekman transport anomaly are shown with color and vector. The NEAMS sea-level distribution derived from satellite altimetry observations during the periods (**c**) H and (**d**) L.

The positive sea-level anomaly by Ekman transport in the southern NEAMS can cause the sea-level anomaly of the NEAMS to be positive because the high sea-level in the southern NEAMS generates more water transport (onshore transport) from the Pacific Ocean (open ocean) to the YS and EJS (marginal sea). This is due to the high water pressure in the southern NEAMS as shown in Figure 6a,c in the period H. The negative sea-level anomaly by Ekman transport in the southern NEAMS can cause the sea-level anomaly of the NEAMS to be negative because the low sea-level in the southern NEAMS causes less water transport from the Pacific Ocean to the YS and EJS. This is due to low water pressure in the southern NEAMS as shown in Figure 6b,d.

There is a strong relationship between wind stress (Ekman transport) and sea-level in the NEAMS as shown in Figure 6; thus, we have determined the area where a maximum correlation is observed between wind stress and sea-level in the NEAMS in Figure 7. The maximum correlation existed in the south of Japan, which was selected as a wind index area (WA). The correlation coefficient between the area averaged wind stress in WA and ANSA is 0.73 (p-value < 0.01, Figure 8). Based on this finding, we can estimate the sea-level anomaly in the NEAMS with wind stress in the WA in August.

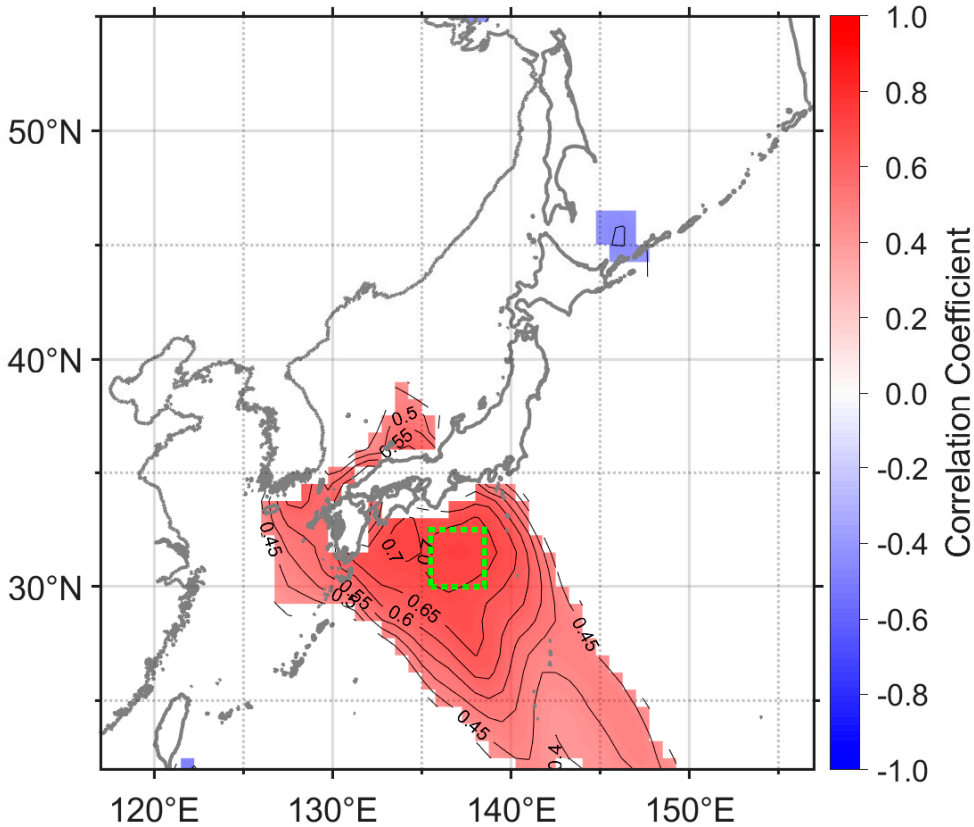

Figure 7. Correlation map of the NEAMS August sea-level with the northwestward (main wind direction in August in the NEAMS) surface wind stress from 1993 to 2018. The contour interval is 0.05 and confidence levels less than 95% were eliminated. A positive correlation means that high NEAMS sea-level occurs with strong northwestward wind stress and a negative correlation means that high NEAMS sea-level occurs with weak northwestward wind stress. Here, the wind index area (WA) showing the maximum positive correlation coefficients is marked with a green dotted box.

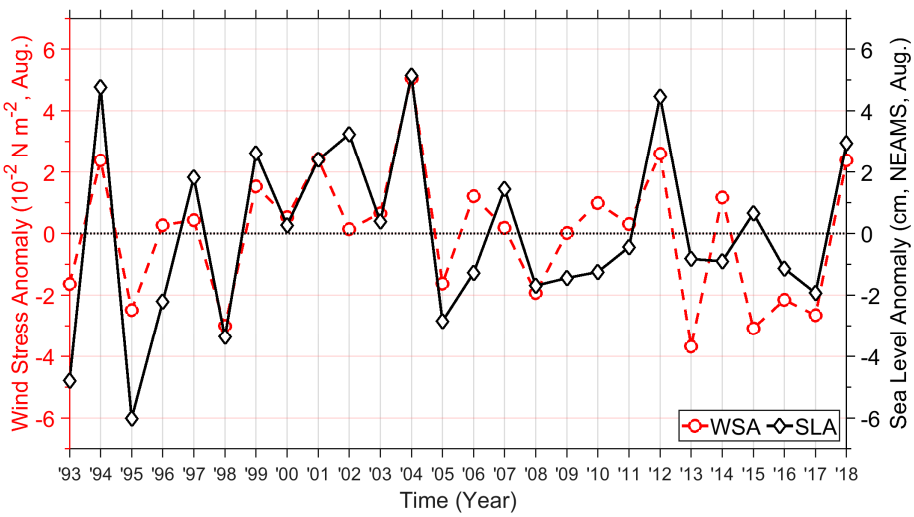

Figure 8. Time-series of area averaged northwestward wind stress anomaly in the WA (red dashed line, left y-axis), and August NEAMS sea-level anomaly observed from satellite altimetry (black line, right y-axis) from 1993 to 2018. The correlation coefficient is 0.73 with p-value < 0.01.

3.4. Atmospheric Pressure Distribution

The wind stress is caused by atmospheric pressure distribution; thus we have examined the correlations between atmospheric pressure in each area and mean sea-level in the NEAMS in August for over 26 years in Figure 9. Positive correlation means that high NEAMS sea-level occurs with high atmospheric pressure and negative correlation means that high NEAMS sea-level occurs with low atmospheric pressure. The areas showing the maximum and the minimum correlation coefficients are Kuroshio Extension (KE) and west of Taiwan (WT) (right and left magenta dotted boxes, respectively in Figure 9). We selected these two areas to define the index, August NEAMS sea-level index (ANSI).

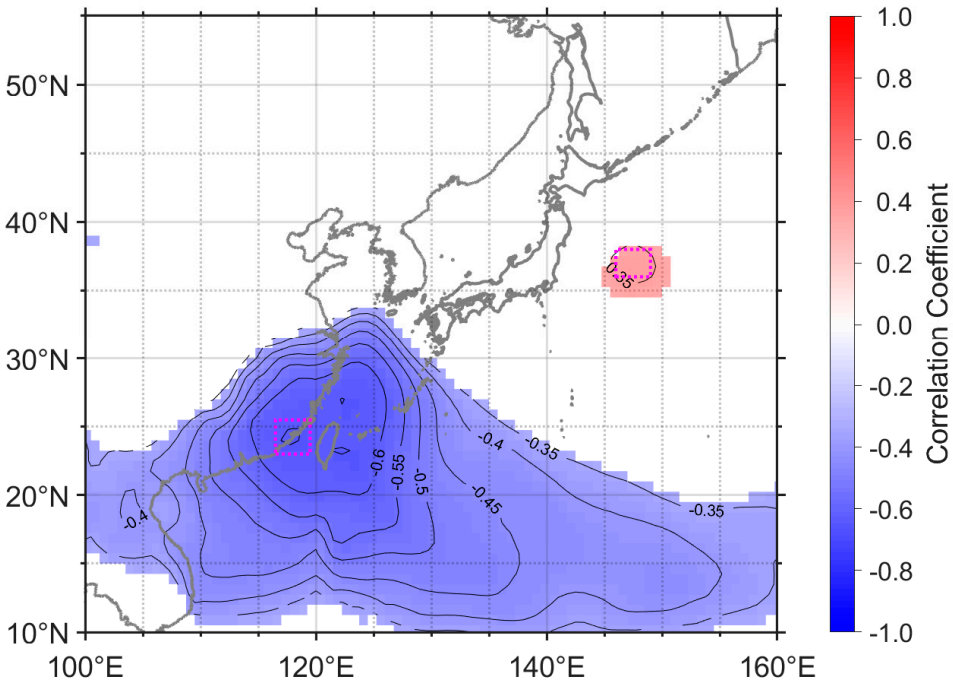

Figure 9. Correlation map of the NEAMS August sea-level with the mean sea-level atmospheric pressure from 1993 to 2018. The contour interval is 0.05 and confidence levels less than 90% were eliminated. Positive correlation means that high NEAMS sea-level occurs with high atmospheric pressure and negative correlation means that high NEAMS sea-level occurs with low atmospheric pressure. The areas showing the maximum (Kuroshio Extension (KE)) and minimum (west of Taiwan (WT)) correlation coefficients are marked with magenta dotted boxes to make the index, August NEAMS sea-level index (ANSI).

There are large atmospheric pressure gradients between high pressure in the KE and low pressure in the WT in the period H in Figure 10a. Large atmospheric pressure gradients result in strong west-northwestward wind stresses. Strong west-northwestward wind stresses cause more north-northeastward Ekman transport from the northwest Pacific Ocean into the NEAMS as shown in Figure 6a,c. There are small atmospheric pressure gradients in areas between high pressure in the KE and low pressure in the WT in the period L in Figure 10b. Small atmospheric pressure gradients result in weak west-northwestward wind stresses. Weak west-northwestward wind stresses cause less north-northeastward Ekman transport from the northwest Pacific Ocean into the NEAMS as shown in Figure 6b,d.

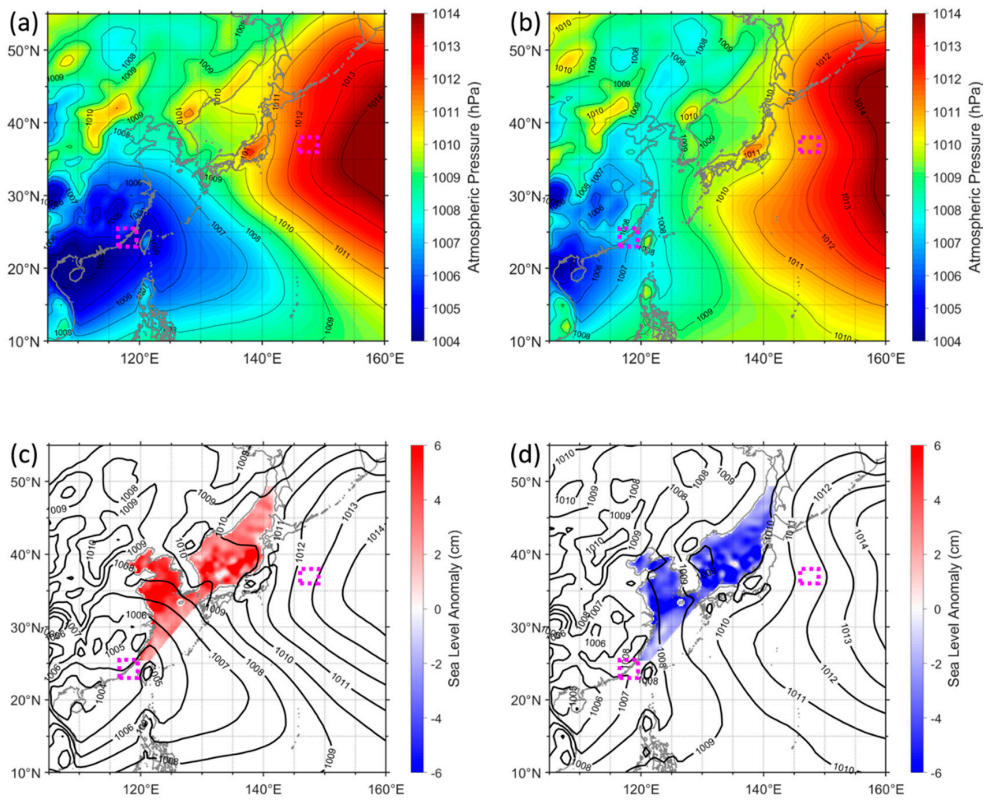

Figure 10. Atmospheric pressures in August averaged for the periods (**a**) H and (**b**) L in the northwest Pacific Ocean (contour intervals: 1 hPa). Atmospheric pressure contours with the colored August NEAMS sea-level anomaly (ANSA) (red: positive, blue: negative) for the periods (**c**) H and (**d**) L. The areas defining the August NEAMS sea-level index (ANSI) are denoted by the magenta dotted boxes, the same as in Figure 9. Coastlines are drawn in grey.

4. Discussion

The sea-level variation by wind has been previously investigated in the NEAMS [8,9,11,27,28]. The surface wind stress is considered as one of the most important factors to change sea-level. The monthly mean sea-levels in the NEAMS have an annual maximum in August, between the years 1993 and 2018. Even though there are other causes for sea-level variability, such as surface heat flux, air and sea surface temperatures, and geostrophic advection [13], the correlations of ANSA with wind stress and atmospheric pressure distribution were significant.

If we define the ANSI as the difference of atmospheric pressure anomalies between the KE (146.0–149.0° E, 36.0–38.0° N) and the WT (116.5–119.5° E, 23.0–25.5° N), the correlation coefficient between ANSI and ANSA is 0.73 (p-value < 0.01) (Figure 11a). Thus ANSA can be estimated quantitatively with ANSI.

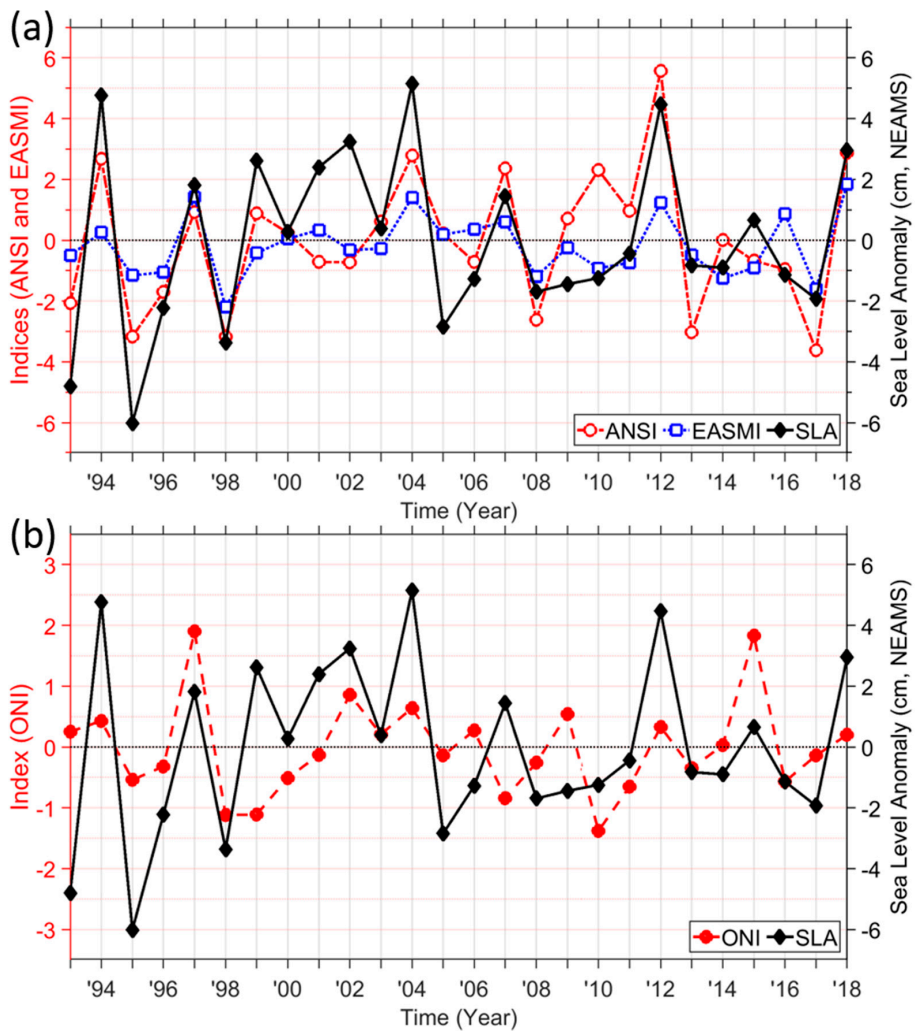

Figure 11. (**a**) Time-series of the ANSI (red dash-dotted line, left y-axis), the East Asian summer monsoon index (EASMI) (blue dotted line, left y-axis), and the ANSA (black solid line, right y-axis) in August from 1993 to 2018. The correlation coefficients between ANSA and ANSI, and ANSA and EASMI are 0.73 (p-value < 0.01) and 0.64 (p-value < 0.01), respectively. (**b**) Time-series of the Oceanic Niño Index (ONI) (red dashed line, left y-axis) and the ANSA (black solid line, right y-axis) and in August from 1993 to 2018. The correlation coefficient between ANSA and ONI is 0.35 (p-value < 0.09).

We compared ANSA and ANSI with other climate indices. The climate indices used in this study were the Aleutian low pressure index (ALPI, [29]), the Arctic Oscillation Index (AOI, [30]), the East Asian summer monsoon index (EASMI, [31]), the North Pacific gyre oscillation (NPGO, [32]), the North Pacific index (NPI, [33]), the Oceanic Niño index (ONI, [34]), the Pacific decadal oscillation (PDO, [32]), and the Siberian high index (SHI, [35]) from 1993 to 2018. The ALPI was only compared with ANSA and ANSI for the years between 1993 and 2015. There are significant correlations between ANSA and EASMI, and ANSI and EASMI, and their correlation coefficients are 0.64 (p-value < 0.01) and 0.69 (p-value < 0.01) (Figure 11a), respectively. This suggests that the August NEAMS atmospheric pressure distribution and East Asian summer monsoon are well related, and the NEAMS sea-level changes in August are correlated with the East Asian summer monsoon. ANSI is slightly better than EASMI in estimating ANSA. The relationship between ANSI and ANSA (correlation coefficient, 0.73 with p-value < 0.01) can be expressed using Equation (2):

$$\text{ANSA (cm)} = 0.92 \times \text{ANSI (hPa)} \quad (2)$$

However, correlations of ANSA and ANSI with other climate indices (ALPI, AOI, NPGO, NPI, ONI, PDO, SHI) were not significant with p-value < 0.05. The correlation between ANSA and ONI is 0.35 (p-value < 0.09), which means there is a weak teleconnection between the NEAMS sea-level and central Pacific Ocean sea surface temperature in August. It implies that the NEAMS sea-level in August might be roughly estimated by El Niño and La Niña (Figure 11). There were more typhoons in August which passed the NEAMS for period H than period L. This may be because of atmospheric pressure distribution, and its cause and effect needs to be investigated more in the near future.

A correlation map of the August sea-level with the ANSI from 1993 to 2018 around the NEAMS was plotted to determine if the ANSI can reproduce the sea-level figures well (Figure 12). A positive correlation indicates that high sea-level occurs with the positive ANSI. The sea-levels of NEAMS areas are highly correlated with ANSI except for in some areas where there are strong currents such as the Kuroshio, and the Taiwan and the Tsushima Warm Currents in the southern part of the NEAMS, and the East Korea and the Tsushima Warm Currents in the southern EJS. This means that the ANSI can be used in estimating the NEAMS sea-level anomaly, but may not be available in strong current and active mesoscale eddy regions. The northern EJS had a higher correlation than those in the YS and around the KS.

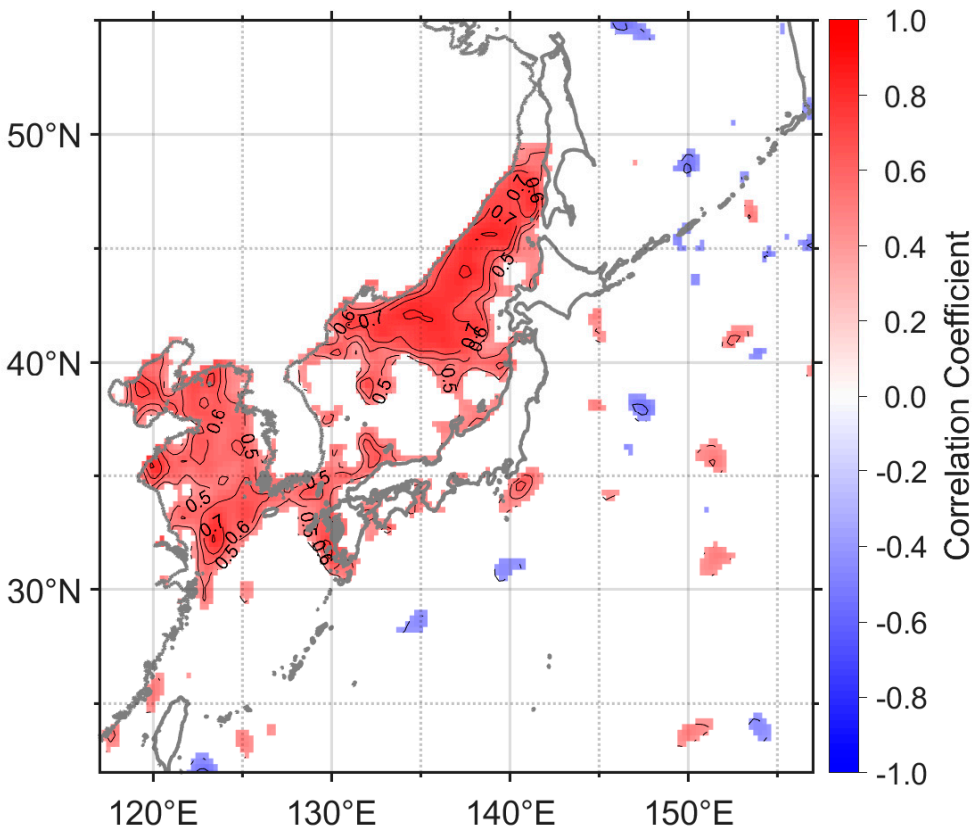

Figure 12. Correlation map of the August sea-level with the ANSI from 1993 to 2018. The contour interval is 0.1 and confidence levels less than 95% were eliminated. A positive correlation indicates that high sea-level occurs with the positive ANSI.

Strong wind stress enhances seawater volume transport from the Pacific into the NEAMS by Ekman transport, which results in high sea-levels in the NEAMS during the period H (Figure 13a). Weak wind stress decreases seawater volume transport, which results in low sea-level in the NEAMS during the period L (Figure 13a).

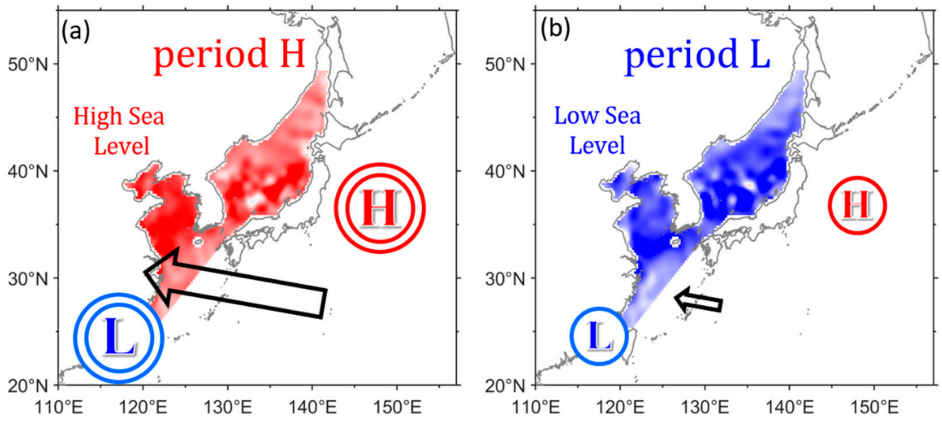

Figure 13. Schematic diagrams accounting for the ANSA. (**a**) Strong west-northwestward wind stress (long black arrow) is a result of large atmospheric pressure gradients (double red and blue circles for H and L, respectively) in the northwest Pacific Ocean. Strong wind stress enhances seawater volume transport from the Pacific into the NEAMS by Ekman transport, which results in high sea-levels in the NEAMS (red) during the period H. (**b**) Weak wind stress (short black arrow) is a result of small atmospheric pressure gradients. Weak wind stress decreases seawater volume transport, which results in low sea-level in the NEAMS (blue) during the period L. Coastlines are drawn in grey.

5. Conclusions

Sea-levels in the NEAMS, between 1993 and 2018, reach annual maxima in August and show remarkable interannual variations. The rising rate of the August sea-level from satellite altimetry data is larger than that of the annual mean in the NEAMS, which itself is larger than that of the global mean sea-level. Thus, it is more important to understand the mechanism of August sea-level change. The interannual variation in August of sea-levels in the NEAMS is dominated by the atmospheric pressure gradients between high pressure in the KE and low pressure in the WT in the south of the NEAMS. In the period H, the ANSA becomes positive due to the large atmospheric pressure gradients between the KE and WT in the south of the NEAMS. In the period L, the ANSA becomes negative due to the small atmospheric pressure gradients between the KE and the WT.

ANSA is mainly determined by the wind stress in the south of the NEAMS and can be estimated quantitatively by ANSI. Local atmospheric forcing (ANSI; local index) may be more influential on ANSA and give a more accurate estimation of sea-levels than remote indices (EASMI, ONI and other indices; climate index) do. Other steric and non-steric effects on sea-level anomalies in August should be considered to estimate ANSA more accurately. Our results spotlight the significant effect of local atmospheric pressure distribution and wind stress on sea-levels in the vicinity of marginal seas. This can be used to estimate sea-levels with atmospheric pressure differences.

Author Contributions: Conceptualisation, M.H. and Y.-K.C.; methodology, M.H., Y.-K.C., H.-W.K., and S.N.; formal analysis, M.H.; investigation, M.H., Y.-K.C. and H.-W.K.; writing—original draft preparation, M.H.; writing—review and editing, M.H. and Y.-K.C.; visualisation, M.H.; supervision, Y.-K.C.; project administration, D.-S.B., K.-Y.J., and E.L.; All authors have read and agreed to the published version of the manuscript.

Funding: This research was a part of the project titled "Analysis and Prediction of Sea Level Change in Response to Climate Change around Korean Peninsula (4)" funded by the Korea Hydrographic and Oceanographic Agency (KHOA), and "Deep Water Circulation and Material Cycling in the East Sea" funded by the Ministry of Oceans and Fisheries (MOF), Republic of Korea. H.-W.K. was supported by KIOST in-house project PE99811.

Acknowledgments: Ssalto/Duacs altimeter products which were produced and distributed by the Copernicus Marine and Environment Monitoring Service (CMEMS) (http://www.marine.copernicus.eu), tide-gauge sea-level data provided by the Permanent Service for Mean Sea Level (PSMSL; http://www.psmsl.org/data/obtaining), and atmospheric pressure and wind-stress data from ECMWF interim reanalysis (http://www.ecmwf.int/) were used in this study.

Conflicts of Interest: The authors declare no conflict of interest.

References

1. Scheffran, J.; Battaglini, A. Climate and conflicts: The security risks of global warming. *Reg. Environ. Chang.* **2011**, *11*, 27–39. [CrossRef]
2. Gill, A.; Niller, P. The theory of the seasonal variability in the ocean. *Deep Sea Res. Oceanogr. Abstr.* **1973**, *20*, 141–177. [CrossRef]
3. Alley, R.B.; Clark, P.U.; Huybrechts, P.; Joughin, I. Ice-sheet and sea-level changes. *Science* **2005**, *310*, 456–460. [CrossRef] [PubMed]
4. Meehl, G.A.; Washington, W.M.; Collins, W.D.; Arblaster, J.M.; Hu, A.; Buja, L.E.; Strand, W.G.; Teng, H. How much more global warming and sea level rise? *Science* **2005**, *307*, 1769–1772. [CrossRef] [PubMed]
5. Lyu, S.J.; Kim, K.; Perkins, H.T. Atmospheric pressure-forced subinertial variations in the transport through the Korea Strait. *Geophys. Res. Lett.* **2002**, *29*, 8-1–8-4. [CrossRef]
6. Nam, S.H.; Lyu, S.J.; Kim, Y.H.; Kim, K.; Park, J.H.; Watts, D.R. Correction of TOPEX/POSEIDON altimeter data for nonisostatic sea level response to atmospheric pressure in the Japan/East Sea. *Geophys. Res. Lett.* **2004**, *31*. [CrossRef]
7. Lyu, S.J.; Kim, K. Subinertial to interannual transport variations in the Korea Strait and their possible mechanisms. *J. Geophys. Res. Ocean.* **2005**, *110*. [CrossRef]
8. Zuo, J.-C.; He, Q.-Q.; Chen, C.-L.; Chen, M.-X.; Xu, Q. Sea level variability in East China Sea and its response to ENSO. *Water Sci. Eng.* **2012**, *5*, 164–174. [CrossRef]
9. Zhang, S.; Du, L.; Wang, H.; Jiang, H. Regional sea level variation on interannual timescale in the East China Sea. *Int. J. Geosci.* **2014**, *5*, 1405. [CrossRef]
10. Yu, K.; Liu, H.; Chen, Y.; Dong, C.; Dong, J.; Yan, Y.; Wang, D. Impacts of the mid-latitude westerlies anomaly on the decadal sea level variability east of China. *Clim. Dyn.* **2019**, *53*, 5985–5998. [CrossRef]
11. Choi, B.-J.; Haidvogel, D.B.; Cho, Y.-K. Interannual variation of the Polar Front in the Japan/East Sea from summertime hydrography and sea level data. *J. Mar. Syst.* **2009**, *78*, 351–362. [CrossRef]
12. Ohshima, K.I.; Simizu, D.; Ebuchi, N.; Morishima, S.; Kashiwase, H. Volume, heat, and salt transports through the Soya Strait and their seasonal and interannual variations. *J. Phys. Oceanogr.* **2017**, *47*, 999–1019. [CrossRef]
13. Amiruddin, A.; Haigh, I.; Tsimplis, M.; Calafat, F.; Dangendorf, S. The seasonal cycle and variability of sea level in the South China S ea. *J. Geophys. Res. Ocean.* **2015**, *120*, 5490–5513. [CrossRef]
14. Noone, K.J.; Sumaila, U.R.; Diaz, R.J. *Managing Ocean Environments in a Changing Climate: Sustainability and Economic Perspectives*; Elsevier: Amsterdam, The Netherlands, 2013.
15. Marcos, M.; Tsimplis, M.N.; Calafat, F.M. Inter-annual and decadal sea level variations in the north-western Pacific marginal seas. *Prog. Oceanogr.* **2012**, *105*, 4–21. [CrossRef]
16. Rio, M.; Guinehut, S.; Larnicol, G. New CNES-CLS09 global mean dynamic topography computed from the combination of GRACE data, altimetry, and in situ measurements. *J. Geophys. Res. Ocean.* **2011**, *116*. [CrossRef]
17. AVISO. MDT; CNES-CLS18. 2020. Available online: https://www.aviso.altimetry.fr/en/data/products/auxiliary-products/mdt.html (accessed on 4 March 2020).
18. Taburet, G.; Pujol, M.-I. Sea Level TAC-DUACS Products. 2020. Available online: https://resources.marine.copernicus.eu/documents/QUID/CMEMS-SL-QUID-008-032-062.pdf (accessed on 30 March 2020).
19. Sealevel_GLO_PHY_L4_REP_Observations_008_047. Available online: Ftp://my.cmems-du.eu/Core/SEALEVEL_GLO_PHY_L4_REP_OBSERVATIONS_008_047 (accessed on 4 March 2020).
20. CMEMS. Global Ocean Gridded L4 Sea Surface Heights and Derived Variables Reprocessed (1993-Ongoing). 2020. Available online: http://marine.copernicus.eu/services-portfolio/access-to-products/?option=com_csw&view=details&product_id=SEALEVEL_GLO_PHY_L4_REP_OBSERVATIONS_008_047 (accessed on 4 March 2020).
21. Holgate, S.J.; Matthews, A.; Woodworth, P.L.; Rickards, L.J.; Tamisiea, M.E.; Bradshaw, E.; Foden, P.R.; Gordon, K.M.; Jevrejeva, S.; Pugh, J. New data systems and products at the permanent service for mean sea level. *J. Coast. Res.* **2013**, *29*, 493–504. [CrossRef]
22. PSMSL. Tide Gauge Data. 2020. Available online: http://www.psmsl.org/data/obtaining/ (accessed on 20 January 2020).

23. Mathers, E.; Woodworth, P. Departures from the local inverse barometer model observed in altimeter and tide gauge data and in a global barotropic numerical model. *J. Geophys. Res. Ocean.* **2001**, *106*, 6957–6972. [CrossRef]
24. Wunsch, C.; Stammer, D. Atmospheric loading and the oceanic "inverted barometer" effect. *Rev. Geophys.* **1997**, *35*, 79–107. [CrossRef]
25. Cheney, R.; Miller, L.; Agreen, R.; Doyle, N.; Lillibridge, J. Topex/poseidon: The 2-cm solution. *J. Geophys. Res. Ocean.* **1994**, *99*, 24555–24563. [CrossRef]
26. Isobe, A. The taiwan-tsushima warm current system: Its path and the transformation of the water mass in the East China Sea. *J. Oceanogr.* **1999**, *55*, 185–195. [CrossRef]
27. Liu, X.; Liu, Y.; Guo, L.; Rong, Z.; Gu, Y.; Liu, Y. Interannual changes of sea level in the two regions of East China Sea and different responses to ENSO. *Glob. Planet. Chang.* **2010**, *72*, 215–226. [CrossRef]
28. Li, Y.; Zuo, J.; Lu, Q.; Zhang, H.; Chen, M. Impacts of wind forcing on sea level variations in the East China Sea: Local and remote effects. *J. Mar. Syst.* **2016**, *154*, 172–180. [CrossRef]
29. Surry, A.; King, J.R. *A New Method for Calculating ALPI: The Aleutian Low Pressure Index*; Fisheries and Oceans Canada, Science Branch, Pacific Region, Pacific Biological Station: Nanaimo, BC, Canada, 2015.
30. Rigor, I.G.; Wallace, J.M.; Colony, R.L. Response of sea ice to the Arctic Oscillation. *J. Clim.* **2002**, *15*, 2648–2663. [CrossRef]
31. Li, J.; Zeng, Q. A unified monsoon index. *Geophys. Res. Lett.* **2002**, *29*, 115-111–115-114. [CrossRef]
32. Di Lorenzo, E.; Schneider, N.; Cobb, K.M.; Franks, P.; Chhak, K.; Miller, A.J.; McWilliams, J.C.; Bograd, S.J.; Arango, H.; Curchitser, E. North Pacific Gyre Oscillation links ocean climate and ecosystem change. *Geophys. Res. Lett.* **2008**, *35*. [CrossRef]
33. Trenberth, K.E.; Hurrell, J.W. Decadal atmosphere-ocean variations in the Pacific. *Clim. Dyn.* **1994**, *9*, 303–319. [CrossRef]
34. Hafez, Y. Study on the relationship between the oceanic nino index and surface air temperature and precipitation rate over the Kingdom of Saudi Arabia. *J. Geosci. Environ. Prot.* **2016**, *4*, 146. [CrossRef]
35. Wu, B.; Wang, J. Winter Arctic oscillation, Siberian high and East Asian winter monsoon. *Geophys. Res. Lett.* **2002**, *29*, 3-1–3-4. [CrossRef]